Simultaneous Size and ζ-Potential Measurements of Individual Nanoparticles in Dispersion Using Size-Tunable Pore Sensors

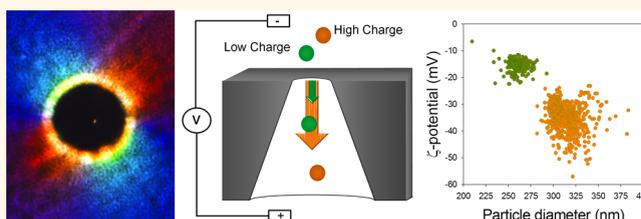**Darby Kozak,[†,*] Will Anderson,[†] Robert Vogel,[‡] Shaun Chen,[†] Fiach Antaw,[†] and Matt Trau[†,§,*]**

[†]Australian Institute for Bioengineering and Nanotechnology, [‡]School of Mathematics and Physics, and [§]School of Chemistry and Molecular Biosciences, University of Queensland, Brisbane, Australia 4072

Characterizing the size and surface charge (ζ-potential) of particulates is important to a wide range of applications and industries where nanoscale colloidal systems are employed. Current characterization methodologies typically rely on ensemble measurements that measure size and charge based on the average mobility of the suspension. Although capable of analyzing a large spectrum of materials and media, ensemble techniques are also inherently biased by small subpopulations.[1] Thus, there has been renewed interest in single particle analysis techniques, such as resistive pulse sensors[2−6] for more accurate dispersion property measurements.[7,8] This sensing technique, which is based on the *Coulter principle*, has been used to characterize the size and concentration of objects from the micrometer to molecular scale, as well as infer information about their charge,[8−11] shape,[12−14] and conductivity.[15]

Although promising measurement devices, a major limitation of most resistive pulse sensors are their fixed pore size, which dictates the size range of objects that can be accurately analyzed.[9,16] In contrast, size-tunable pore sensors have the advantage of tuning the pore dimensions, via hydrodynamic focusing,[17] mechanically stretching elastic pores,[18] or coating pores with dynamic lipid bilayers, to the particulate system at hand.[19] Tuning the pore size increases the analysis size range, improves measurement sensitivity, and can be used to selectively gate larger objects from analysis.[20] Previous studies have used elastic, size-tunable, pores to measure the size[21] and concentration[22] as well as infer information about the charge[23,24] of synthetic and biological particle suspensions. Recently, we developed an empirical

ABSTRACT

The prospect of characterizing individual nanoparticles, molecules, or DNA base pairs has generated considerable interest in resistive pulse sensing. In addition to size and concentration analysis, this technique also has the capacity to measure the charge density of objects in situations where electrophoretic forces dominate their motion. Here we present a methodology to simultaneously extract, *via* appropriate theoretical models, the size and ζ-potential of objects from the resistive pulse signal they generate. The methodology was demonstrated using a size-tunable elastic pore sensor to measure a complex "bimodal" suspension composed of two particle sets with different size and charge. Elastically tuning the size of the pore sensor, by stretching the elastic pore membrane, enables a larger sample size range to be analyzed, improves measurement sensitivity, and fine-tunes the forces acting on objects. This methodology represents a new approach for investigating and understanding the fundamental behavior of nanoscale dispersions.
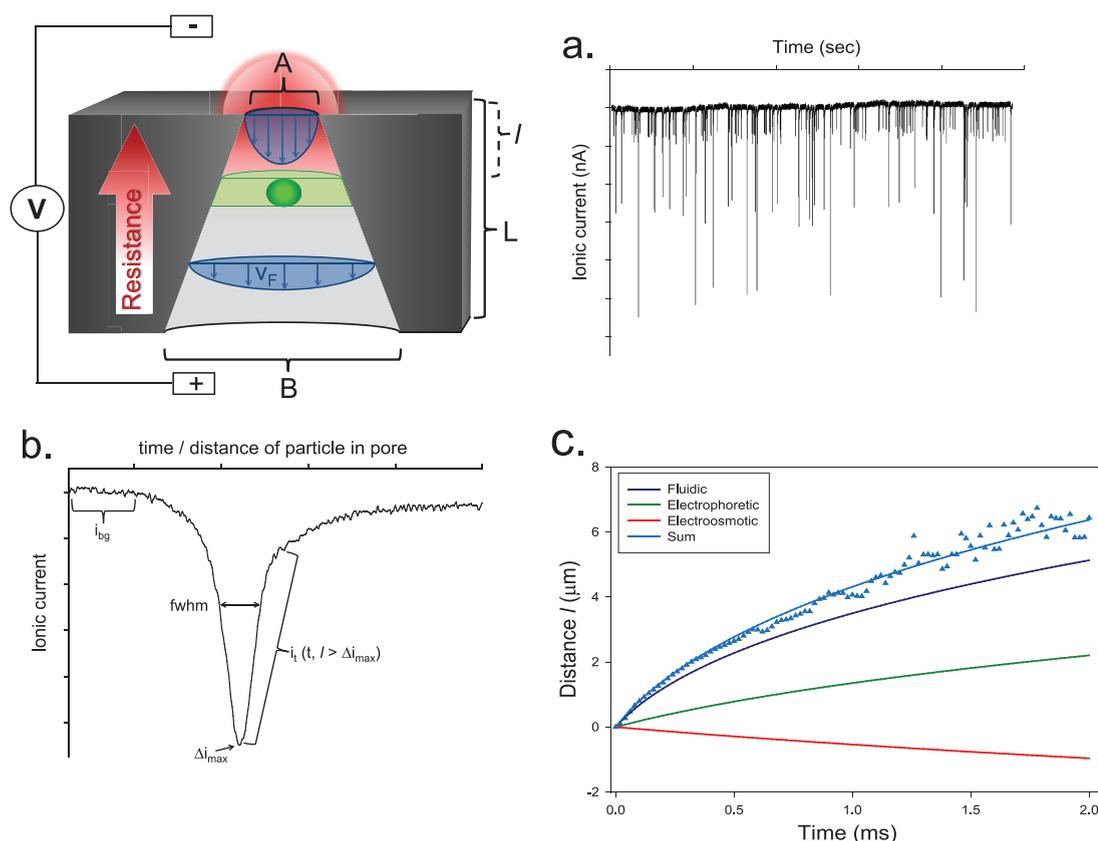
model to describe how the elastic pore dimensions change with applied stretch, and when used in combination with a simplified resistance model, we demonstrated the ability to measure both the size and velocity profile of individual particles traveling through the conically shaped pore.[25] As particle velocity in pore sensors is dependent on the particle's charge, these findings and those by Lan *et al.*[26] indicate that the magnitude and shape of the generated pulse signals can be used to simultaneously

Figure 1. Illustration of a conical pore sensor with length L and small and large opening diameters of A and B. The pore geometry gives rise to a resistance gradient (red gradient) and fluid velocity profile (v_F, blue arrows) through the pore, which is highest at the small pore opening. Also shown is a particle (green circle) and the corresponding excluded local volume fraction of the particle at a distance l into the pore. (a) Ionic current "pulses" in time (i_t) generated by individual particles passing through the elastic pore sensor. (b) Close up of a single i_t pulse peak labeled with characteristic measurement features being background current (i_{bg}), maximum change in current pulse signal (Δi_{max}), and the full width at half-maximum pulse duration (fwhm). Also shown in the bracket is the portion of the pulse signal corresponding to the particles position in the pore ($i_t > \Delta i_{max}$) that was used to calculate the position-in-time ($l(t)$) of individual particles traversing the pore. (c) Typical experimental $l(t)$ trace of a particle (symbols) and corresponding theoretical electrophoretic, electroosmotic, and fluidic model contributions to the particle position-in-time. Data shown are for a 330HC particle traversing the pore at 324 Pa, 0.38 V, a membrane charge of -8 mV, and calculated ζ-potential of -15.9 mV.

measure both the size and ζ-potential of individual particles.

Herein we present a simple methodology to simultaneously measure the size and ζ-potential of individual particles using a conically shaped elastic pore sensor. The simplified resistance model presented in this study enables both particle size and position-in-time (velocity) to be elucidated from the resistive pulse signal. Single particle ζ-potentials were calculated by fitting the experimental position-in-time data to the sum of the theoretical forces acting on particles in the pore, being electrophoresis, electroosmosis, and fluidic. Varying the pore size, voltage, and pressure was used to control the magnitude of the forces driving particle translocation. translocation. Although demonstrated on a size-tunable conical pore, the presented methodology can potentially be applied to any pore sensor of known geometry.

RESULTS AND DISCUSSION

Elastic pore sensors are conically shaped, size-tunable pores that are fabricated by puncturing a polyurethane

thermoplastic membrane with a tungsten needle.[18] Stretching or relaxing the elastic membrane enables the dimensions of the conical pore (Figure 1) to be altered or "tuned" to the size range of the particulate sample. In this study, stretching the membrane from 45 to 52 mm increased the diameter of the small (A) and large (B) pore openings and decreased its length (L) by 0.56–0.97, 32.7–57.2, and 231–171 μm, respectively. These dimensions were measured according to our previously described methodology using the ionic current, optical microscopy, and a caliper micrometer.[25]

When a voltage is applied across the conical pore, its shape results in a resistance gradient that is highest at A.[27] Objects are detected in these pores as a change in the resistance (ΔR) across the pore, which is proportional to local excluded volume of the object, as shown in the schematic of Figure 1. The magnitude of the ΔR signal is therefore dependent on both the size and position of the particle in the pore.[27] Particle size d and distance l from the small pore opening (position) are related to the pore dimensions (A, B, and L)

and ΔR by

$$\Delta R = \frac{4\rho d^3}{\pi\left(A + I\left(\dfrac{B-A}{L}\right)\right)^4} \qquad (1)$$

where ρ is the resistivity of the media, and in this study, ΔR was measured via the change in the ionic current-in-time (i_t) by

$$\Delta R = \left(\frac{V}{i_t} - \frac{V}{i_{bg}}\right) \qquad (2)$$

where V is the applied voltage and i_{bg} is the background current through the pore when no particle is present.

This model of the ΔR signal approximates the conical pore as a series of cylindrical pore sections of increasing diameter and applies the Maxwell formula[9,16,28] to each of these sections. Modeling the pore in this manner slightly under-predicts the magnitude of ΔR generated by a particle. However, it does provide a simplified means of calculating both particle size and position. Resistance models which also incorporate the resistance gradient across the particle diameter, such as that proposed by Heins et al.,[27] should more accurately reflect the ΔR signal. However, solving for the particle size and position becomes a nontrivial matter.

In this study, particle size was calculated by rearranging eq 1 to solve for d and from the assumption that $i_t = \Delta i_{max}$ when $I = 0$. In other words, Δi_{max} occurs when the particle blocks the greatest amount of electrolyte ion flux through the pore, which is at A. From this assumption, the position of the particle in the pore is calculated from the measured particle diameter and the magnitude of i_t at times other than Δi_{max} by rearranging eq 1 to now solve for I. Thus each point on the i_t trace can be used to calculate the distance a particle travels in a given amount of time (Figure 1c). In this study, only times greater than Δi_{max} were used to calculate particle position, as this corresponds to when the particle was located within the defined boundary conditions inside the pore. Furthermore, as each i_t pulse corresponds to a single particle, the collation of hundreds to thousands of pulses, which can be achieved over a short (i.e., seconds) analysis duration (Figure 1a), enables not only particle-by-particle characterization but also analysis of the overall distribution of the suspension.

Modeling Forces Acting on Particle Translocation. The velocity of a particle (v_p) traveling through a resistive pulse sensor is typically due to a combination of electrophoretic (v_E), electroosmotic (v_O), and fluidic (v_F) velocities, such that $v_p = v_E + v_O + v_F$.[9] Although present, Brownian motion (e.g., diffusion) is typically considered to be negligible within the pore due to the magnitude of the other forces. Thus, $v_p = v_E$ in pore

sensors designed so that electroosmotic and pressure forces are negligible. DeBlois et al.[9] and later Ito et al.[8,11] used this relationship to correlate v_E, and thus particle ζ-potential, to the time it took particles to pass through a horizontally orientated cylindrical pore of known length. This correlation is possible for cylindrical pores without surface charge or applied pressure due to the homogeneous electric field through the pore. In contrast, conically shaped pores that have surface charge and use an applied pressure to increase particle translocation give rise to gradients in v_E, v_O, and v_F acting on particle translocation. Although more complex, these gradients, and their contribution to v_p, can be described by the conservation of the electric field Φ and momentum τ flux using finite-element computer simulation packages[26,29] or by the simplified methodology presented below. It is important to note that increasing the applied voltage and/or pressure will increase the magnitude of v_E, v_O, and v_F but does not change their profiles through the pore. This is solely dependent on the pore geometry.

From the conservation of momentum, the average v_F through a channel/pore is proportional to the volumetric flow rate (Q) divided by the cross sectional pore area ($\langle v_F \rangle = Q/\pi r^2$). Recently Lan et al.[29] and Roberts et al.[22] used the Hagen−Poiseuille equation to derive the expected Q through a conical nanopore. They used the geometric relationship between pore radii and I to show that Q is dependent on the pore angle and inversely proportional to the difference between the third powers of the small and large pore opening radii. When the radius of the large pore opening ($B/2$) is at least an order of magnitude larger than the small ($A/2$), this complex relationship simplifies to

$$Q = \frac{3\pi A^3 \Delta P}{128\eta\left(\dfrac{L}{B-A}\right)} \qquad (3)$$

where η is the solution viscosity and ΔP is the pressure drop across the pore, which is approximately 75% of the total applied pressure (Figure 2S in Supporting Information).[29]

To assess the validity of the conical fluid model, we compared the theoretical value of A calculated from the linear relationship between Q and ΔP to the experimental value of A, calculated from optical microscopy and the ionic current measurements through the pore. To achieve this, Q values were measured from the particle event frequency for multiple particle dilutions with increasing pressure, as shown in Figure 3S and as discussed in greater detail in the Supporting Information. The theoretical value of A (0.888 μm) calculated from eq 3 showed good correlation to the experimental A value (0.95 μm), being within 6.5% ($\sim$0.06 μm) of each other.

Interestingly, it was also found that the vertical fluid cell setup in our qNano system gave rise to an inherent

pressure head of 28 Pa, corresponding to a fluid height of 0.28 cm, when 40 μL of sample was added. This can be seen from the greater than 0 intercept in the plot of Q versus ΔP (Figure 3S in the Supporting Information). Vogel et al.[24] observed a similar but slightly higher pressure head of 40−50 Pa when 40 μL of sample was added. As this inherent pressure head acts on particles traveling through the pore, 28 Pa was added to ΔP values used in calculations of v_F, as discussed below.

Theoretical modeling of the electrophoretic, electroosmotic, and fluidic forces enables the contribution that each of these forces plays on particle translocation through the pore to be elucidated. The high ionic concentration, and therefore short Debye lengths ($\kappa^{-1} \ll$ than the particle or pore diameters) typically present in pore sensors, means that v_E and v_O are, respectively, proportional to the ζ-potential of the particle (ζ) and pore wall (ψ), according to the Smoluchowski equation.[30] For conical pores, in which the pore diameter increases as a function of l, the magnitudes of v_E, v_O, and v_F are highest at A and inversely proportional to l^2. By integrating these velocity terms with respect to time (t), their contribution on particle position in the pore is calculated by the sum of the electrophoretic, electroosmotic, and fluidic $l(t)$ terms, where

$$l(t) = \left(\frac{L}{B-A}\right)\left(\left(\sqrt[3]{\left(\frac{B-A}{L}\right)D + A^3}\right) - A\right) \quad (4)$$

and the D terms are respectively

$$D = \frac{3\varepsilon\zeta VAB}{L\eta}t, \quad \frac{3\varepsilon\psi VAB}{L\eta}t, \quad \text{or} \quad \frac{9A^3\Delta P}{32\eta\left(\frac{L}{B-A}\right)}t$$

for the electrophoretic, electroosmotic, and fluid flow component to particle position, and ε is the dielectric constant ($\varepsilon = \varepsilon_o\varepsilon_r$) of the aqueous media. Derivations of all these equations are provided in the Supporting Information.
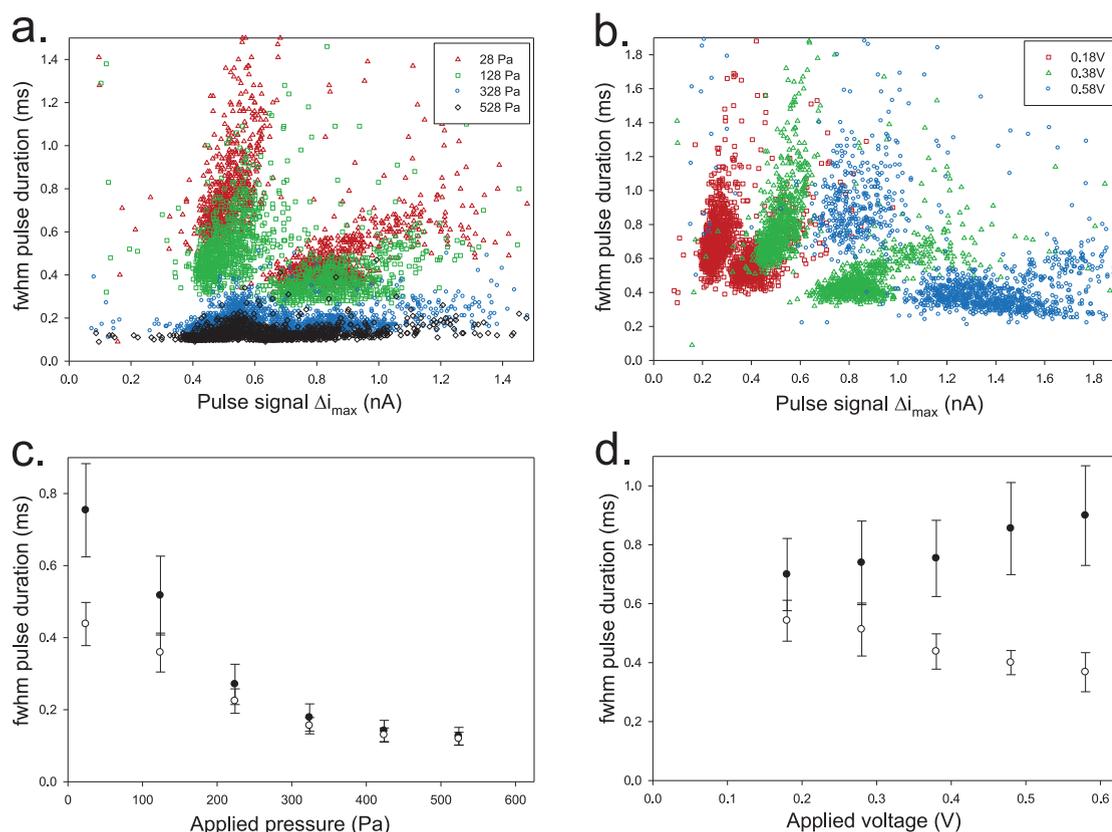
Therefore, as shown in Figure 1c, the ζ-potential of a particle can be calculated from a conical pore sensor of known geometry, ΔP and ψ, by fitting the experimental particle position-in-time trace to the sum of the theoretical electrophoretic, electroosmotic, and fluid $l(t)$ terms. It should be noted that the direction of the electrophoretic and electroosmotic forces are dependent on the sign of voltage, ζ and ψ.

Measuring Particle Suspensions with Bimodal Size and Charge. The ability to measure both the size and ζ-potential of individual particles *via* the generated pulse signals was demonstrated on a mixed bimodal particle suspension. The suspension was composed of an equal mixture of two polystyrene particle populations, 300LC and 330HC, that were 296 and 335 nm in size and had, respectively, low (−12 ± 3 mV) and high (−34 ± 6 mV) surface charge. Particle size and

ζ-potential values given here were measured by dynamic and phase analysis light scattering (DLS and PALS), respectively, and are used as a standard for comparison. Particles were suspended in an electrolyte buffer (EB) composed of 100 mM KCl, 10 mM Tris, and 0.01% Tween 20, pH 7.5, that at 25 °C had a measured resistivity and viscosity of 0.775 ± 0.012 Ω m and 0.9 cP.

In general, studies characterizing objects using resistive pulse sensors only report the Δi_{max} and duration of the generated pulse signal (Figure 1b). As discussed before, these provide qualitative information and an easy means to compare the relative size and velocity of detected objects. They also provide an easy means to evaluate the sensor's ability to distinguish between similarly sized and charged objects, such as those examined in this study, while also demonstrating how system parameters, such as applied pressure and voltage, influence the pulse signal and detection limitations. In this study, the resistive pulse signals generated by individual particles within the bimodal suspension gave rise to two distinct Δi_{max} versus duration signal populations at low applied pressures (less than ~250 Pa) and all voltages examined (Figure 2a,b), indicating that the signal sensitivity is sufficient enough to distinguish between the two similar particle sets.

Increasing the applied pressure reduced the time it took particles to traverse the pore, as shown by the decreased pulse signal duration (millisecond), measured here at the full width at half maximum (fwhm). However, it did not alter Δi_{max}, which were ~0.5 and ~0.8 nA for the 300LC and 330HC particles, respectively. This is because pressure affects the fluid flow but not the resistance gradient through the pore. Thus increasing the applied pressure, and therefore the magnitude of v_F acting on the particle, reduces only the pulse signal duration. As shown in Figure 2a,b, increasing pressure to greater than ~250 Pa resulted in the two particle populations going from two distinguishable signal populations to a single overlapping fwhm signal at 0.175 ms. This is better demonstrated from the plot of the average fwhm values of the two particle sets with pressure (Figure 2c). Average fwhm values for each particle population were determined by gating using the Δi_{max} of the raw bimodal data presented in Figure 2a. For example, in the pressure experiments, pulses with a Δi_{max} below or above ~0.6 nA were attributed to the 300LC or 330HC particle population, respectively. Increasing pressure clearly shows a corresponding decrease in the fwhm durations for both particle sets. At pressures greater than ~250 Pa, their signals converge, indicating that v_F dominates particle translocation. Below ~250 Pa, the 300LC particles had a larger fwhm duration than that observed for the 330HC particles; that is, the lower charge 300LC particles took longer to traverse the pore. This indicates that electrophoretic and/or

Figure 2. Pressure and voltage affects on particle pulse signal. Collating the fwhm duration and Δi_{max} of all individual particle pulses shows particle population trends and distributions. Plots of the fwhm duration against Δi_{max} (*i.e.*, ~particle velocity *vs* size) generated by individual particles in a mixed "bimodal" suspension of 300LC and 330HC particles. (a) Appling pressure to the system (28–528 Pa) reduced the particle translocation time (fwhm) but did not affect the Δi_{max} signal. (b) Increasing the applied voltage (0.18–0.59 V) increased the fwhm *vs* Δi_{max} signal separation between the two particle sets, as applied voltage is proportional to both the magnitude of the pulse signal and the electrophoretic driving force acting on the particle. The fwhm average and standard deviation of the 300LC (●) and 330HC (○) particles, from panels a and b, with increasing applied (c) pressure and (d) voltage. Fluid forces acting on particle translocation dominate at pressures greater than ~250 Pa, demonstrated by the similar fwhm for both particle sets.
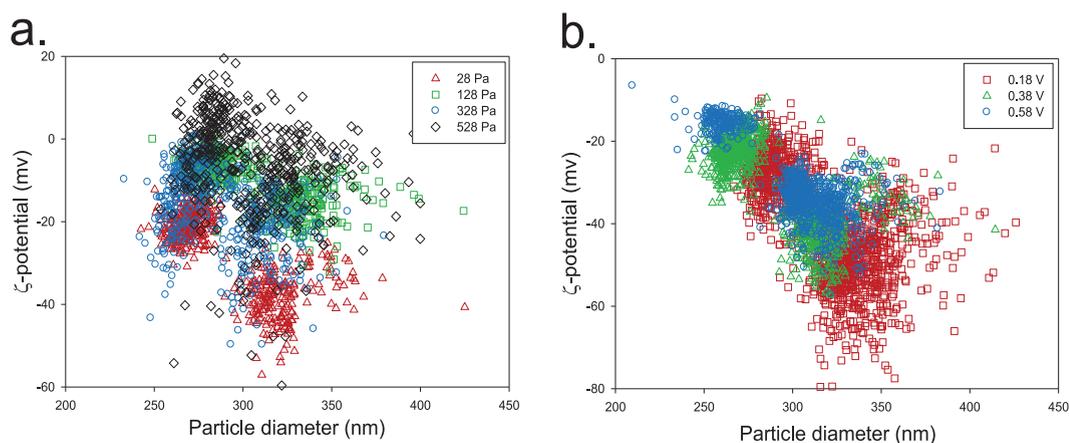
electroosmotic forces become appreciable at pressures below 250 Pa.

Increasing the applied voltage from 0.18 to 0.58 mV was found to proportionally increase both Δi_{max} and the difference in fwhm durations measured for the two particle sets. This gave rise to an increase in the signal separation and therefore discrimination between the two particle populations. As demonstrated by eqs 2 and 4, increasing the voltage is expected to give rise to larger Δi_{max} values as well as v_E and v_O contributions. Thus, the fwhm durations are expected to reduce with increasing voltage. As shown in Figure 2d, this trend was observed for the higher charged 330HC particle set. However, it had the opposite effect on the 300LC particles; for example a slight increase in the fwhm duration was observed at higher voltages. This indicates the existence of electroosmosis in the pore, which is counter to v_E.

Streaming potential measurements, and recent findings by Vogel *et al.*,[24] showed that the elastic polyurethane pore membrane has a negative surface charge (ψ) of approximately -8 ± 3 mV when in

EB. This negative membrane charge gives rise to an electroosmotic force that is counter to the pressure and electrophoretic forces acting on the negatively charged particle sets used in this study. Thus, $v_P = v_E - v_O + v_F$ in this study, and a ψ of -8 mV was used in the electroosmotic model for calculating single particle ζ-potentials.

Tuning the pore dimensions *via* stretching the membrane from 50 to 52 mm, at a constant applied pressure and voltage, was found to decrease both Δi_{max} and the average fwhm, as shown in Figure 4S of the Supporting Information. These decreases in the signal are due, respectively, to the decreased local excluded volume fraction of the particle and increased Q that result from the change in pore dimensions (*e.g.*, larger A, B and shorter L). Although changes in the resistance gradient profile are a possible explanation for the observed shorter fwhm, our previous study indicated that stretching the pore from 42 to 50 mm had minimal to negligible impact on altering the resistance gradient, that is, the "effective" sensing zone length of the pore, which ranged from 27 to 32 μm.[25]

Figure 3. Size and charge distribution of individual particles within the 300LC and 330HC bimodal suspension with increasing (a) applied pressure and (b) voltage. Each data point corresponds to a single particle traversing the pore.

TABLE 1. Size and Velocity Distribution of a Mixed Bimodal Particle Suspension of 300 and 330 nm Polystyrene Particles with Low and High Surface Charge, Respectively, with Increasing Applied Pressure and Voltage

| | | | 300LC particle set | | 330HC particle set | |
| | | | 300 nm, low charge | | 330 nm, high charge | |
condition	applied pressure [Pa]	applied voltage [V]	diameter [nm]	ζ-potential [mV]	diameter [nm]	ζ-potential [mV]
DLS/PALS[a]			296 ± 12	−12 ± 3	335 ± 16	−34 ± 6
pressure 1	28	0.38	268 ± 8.5	−20.6 ± 3.5	320 ± 16	−37.6 ± 5.6
pressure 2	128	0.38	272 ± 10	−5.5 ± 2.9	320 ± 13	−14.5 ± 4.5
pressure 3	228	0.38	275 ± 11	−6.3 ± 5.3	321 ± 13	−15.9 ± 6.4
pressure 4	328	0.38	270 ± 11	−10.1 ± 7.7	313 ± 14	−19.4 ± 9.0
pressure 5	428	0.38	280 ± 11	−6.6 ± 10.1	323 ± 19	−17.2 ± 10.6
pressure 6	528	0.38	284 ± 12	−0.4 ± 9.1	330 ± 23	−12.4 ± 12.3
voltage 1	28	0.18	297 ± 11	−30.7 ± 6.2	345 ± 22	−50.7 ± 10
voltage 2	28	0.28	260 ± 11	−16.8 ± 3.6	305 ± 16	−34.3 ± 6.6
voltage 3	28	0.38	268 ± 8.5	−20.6 ± 3.5	320 ± 16	−37.6 ± 5.6
voltage 4	28	0.48	270 ± 10	−18.4 ± 2.8	322 ± 16	−38.2 ± 6.0
voltage 5	28	0.58	261 ± 10	−15.7 ± 2.5	314 ± 14	−35.0 ± 5.2

[a] DLS/PALS values represent separate, unmixed, single modal measurements of the two particle populations.

Thus, the decreased fwhm is due to the higher v_F through the pore, arising primarily from the increase in A. Size tuning of elastic pore sensors, therefore, has the added advantages over conventional fixed pore sensors of both improving the measurement sensitivity and fine-tuning particle velocity through the pore.

Pulse Signal Analysis for Calculating Individual Particle Size and ζ-Potential. Individual particle size and charge, as well as their distribution in the bimodal suspension, were calculated from the individual pulse signals generated under increasing pressure and voltage (data presented in Figure 2a,b). As discussed previously, particle diameters were calculated from the Δi_{max} signal and the pore geometry using eq 1, and ζ-potentials were calculated by fitting the sum of the electrophoretic, electroosmotic, and fluid $I(t)$ components (eq 4) to the experimental particle position-in-time calculated from eq 1 at times greater than Δi_{max}, as shown in Figure 1c. As expected, and as

shown from the 300LC and 330HC position-in-time traces in Figure 4S of the Supporting Information, increasing the pressure or voltage increased the particle velocity through the pore; that is, they traveled greater distances over the same time period.

As shown in Figure 3a,b, the calculated size and ζ-potentials gave rise to two distinct particle populations at all of the conditions examined. These were centered close to the expected 300LC and 330HC values of 296 nm, −12 mV and 335 nm, −34 mV, as measured by DLS and PALS. The calculated average and standard deviations for the 300LC and 330HC particle sets using the elastic pore sensor at the different pressure and voltage conditions are given in Table 1.

In general, over all conditions studied, the calculated sizes for the 300LC and 330HC particles in the bimodal suspension were ~273 and 321 nm. These sizes had less than 3% variation between experimental conditions and are within 9% of the single modal DLS

measurements. Unlike size calculations, ζ-potential calculations had a higher variance ($\sim$50%) between experimental conditions. Increasing pressure had the greatest effect. The ζ-potentials calculated for the 300LC and 330HC particle populations dropped, respectively, from -20.6 to -0.4 mV and -37.6 to -12.4 mV when the applied pressure was increased from 28 to 528 Pa. This supports the fwhm findings presented in Figure 2c that at higher pressures v_F increasingly dominates particle translocation, which in turn reduces the accuracy of ζ-potential measurements.

From eq 4, the theoretical electrophoretic contribution to particle position goes from $\sim$57 to $\sim$23% as the applied pressure is increased from 28 to 528 Pa. It should be noted that these percentages are calculated from the sum of absolute force contributions over the first 2 μm of the pore using $\zeta = -25$ mV, $\psi = -8$ mV, an applied voltage of 0.38 V, and ΔP, which is 75% of the applied pressure. Additionally, increasing v_p reduces the number of data points that comprise the i_t pulse. Both of these factors reduce the sensitivity and accuracy of calculated ζ-potentials. In contrast, increasing the applied voltage from 0.18 to 0.58 V improved both the calculated size and ζ-potential distributions (Figure 3b). This is due to increased pulse signal-to-noise and theoretical electrophoretic contribution, which goes from $\sim$50 to 60%. As a result, the calculated ζ-potential values had a lower variance than the pressure data and correlated well with the PALS values.

The average calculated ζ-potentials for the 300LC and 330HC particle sets were -13.8 and -28.4 mV, respectively, over all of the experimental conditions examined. These are within 15 and 16% of the single modal PALS measurements, which were -12 and -34 mV. Differences between the light scattering and pulse sensor values are believed to be due to a combination of effects. The first being the uncertainty of DLS and PALS measurements; these ensemble techniques measure an averaged particle size and charge and are biased by particles that scatter more light. The second is the magnitude of the electrophoretic contribution to particle position, as well as the theoretical assumptions and measurement errors involved with the developed conical pore technique, that is, in our cylindrical approximation of ΔR (eq 1) and errors in measuring the pore dimensions and applied pressure. However, as evident by the small 9% difference in sizing and $\sim$16% difference in ζ-potentials, these are minimal.

CONCLUSIONS

As demonstrated in this article, the key to achieving single particle size and charge analysis using a pore sensor is to extract, *via* appropriate theoretical models, the electrophoretic component to particle motion from the generated resistive pulse signal. Our results show that ζ-potential is easily and accurately calculated when electrophoretic mobility dominates the particle velocity through the pore. We were able to control the electrophoretic contribution by varying the applied voltage, pressure, and pore size in our system. Tuning the pore size has the added benefit of improving measurement sensitivity.

Size and ζ-potential analysis of a complex bimodal suspension, composed of two monodisperse polystyrene particle sets, using the described methodology, were within 9 and 16% of single modal DLS and PALS measurements, respectively. Given the simplicity and robustness of this methodology, we believe that it will be of significant interest to the wide-ranging scientific communities where particulate suspensions are used. Furthermore, characterizing dispersion properties on an object-by-object basis, such as demonstrated in this paper, represents a new approach for investigating and understanding the fundamental behavior of biological and synthetic particle suspensions, which is not possible by current ensemble analysis techniques.

MATERIALS AND METHODS

Characterizing the qNano Elastic Pore Sensor. An elastic pore membrane, supplied by IZON Science Ltd. (NZ) and manufactured as described previously,[18] was mounted on the stretching jaws of the qNano (IZON Science) and prestretched by cycling the membrane from 42 to 52 mm of applied stretch 5 times prior to imaging and experimental application. The large pore opening was imaged at 42, 43.5, 45, 47.5, and 50 mm stretches using an IX70 Olympus microscope at 60× magnification. The area of the pore opening was calculated from the image contrast using ImageProPlus software, which was calibrated using a 0.01 mm increment calibration slide. The pore membrane thickness was measured at the center of the membrane using a calliper micrometer. All of the measurements were done in triplicate, and the pore was allowed to relax to 42 mm of stretch between measurements.

Particle Measurements. Carboxyl-modified polystyrene particles of 300 and 330 nm with low (300LC) and high (330HC) surface charge, respectively, were purchased from Bangs Laboratories (USA). The particle ζ-potentials, reported as an average and standard deviation of 3 measurements using a Malvern 300HS, were -12 ± 3 and -34 ± 6 mV, respectively. Particles were dispersed in an electrolyte buffer composed of 100 mM KCl, 10 mM Tris, and 0.01% Tween 20, which had a measured pH of 7.5, resistivity of 0.775 ± 0.012 Ωm, and viscosity of 0.9 cP for all experiments.

For all qNano experiments, 40 μL of the particle suspension was added to the top fluid cell and a minimum of 500 events were recorded for each measurement condition. The analog digital converter operates at 1 MHz, which is reduced to a sampling rate of 50 KHz through electronic filtering. Measurements were done at 50 mm of applied stretch, which corresponded to a large (*B*) and small (*A*) opening diameter of 51.7 and 0.95 μm and a pore length (*L*) of 187 μm. Pressure was applied to the top fluid cell using the Izon Science variable pressure module, which was calibrated against an in-house manometer. Fluid flow rate measurements were conducted at 0.18 V and using 5 concentrations (3.54×10^6, 5.31×10^6, 7.07×10^6,

8.84×10^6, 10.6×10^6 particles μL^{-1}) of the 300LC particles at 5 applied pressures (100, 200, 300, 400, and 500 Pa). Bimodal experiments were conducted on a mixed suspension of the 300LC and 330HC particles with either increasing applied pressure of 0, 100, 200, 300, 400, and 500 Pa (0.38 V) or increasing voltage of 0.18, 0.28, 0.38, 0.48, and 0.58 V (100 Pa). The current pulse signals were collected and exported for analysis using IZON proprietary software V2.0, as well as processed through an in-house "peak extractor and analysis" software program. Average and standard deviation size and ζ-potential values presented in Table 1 were determined by 2D gating of the particle populations using Origin 8.0 software.

Conflict of Interest: The authors declare no competing financial interest.

Supporting Information Available: Optical microscopy images of the large pore opening, details of the finite-element simulation of the fluid velocity profile and pressure drop across the pore, experimental measurements of the fluid flow rate (*Q*), experimental measurements of fluid velocity change with pore size, additional examples of experimental particle position-in-time curves with increasing pressure and voltage, as well as derivations of the electrophoretic, electroosmotic, and fluidic velocity terms. This material is available free of charge *via* the Internet at http://pubs.acs.org.

REFERENCES AND NOTES

1. Merkus, H. G. *Particle Size Measurements: Fundamentals, Practice, Quality*; Springer: Berlin, 2008.
2. Dekker, C. Solid-State Nanopores. *Nat. Nanotechnol.* **2007**, *2*, 209–215.
3. Kozak, D.; Anderson, W.; Vogel, R.; Trau, M. Advances in Resistive Pulse Sensors: Devices Bridging the Void between Molecular and Microscopic Detection. *Nano Today* **2011**, *6*, 531–545.
4. Li, Y.-Q.; Zheng, Y.-B.; Zare, R. N. Electrical, Optical, and Docking Properties of Conical Nanopores. *ACS Nano* **2012**, *6*, 993–997.
5. Zhang, H. P.; Chon, C. H.; Pan, X. X.; Li, D. Q. Methods for Counting Particles in Microfluidic Applications. *Microfluid. Nanofluid.* **2009**, *7*, 739–749.
6. Sexton, L. T.; Horne, L. P.; Martin, C. R. Developing Synthetic Conical Nanopores for Biosensing Applications. *Mol. Bio-Syst.* **2007**, *3*, 667–685.
7. Fraikin, J. L.; Teesalu, T.; McKenney, C. M.; Ruoslahti, E.; Cleland, A. N. A High-Throughput Label-Free Nanoparticle Analyser. *Nat. Nanotechnol.* **2011**, *6*, 308–313.
8. Ito, T.; Sun, L.; Bevan, M. A.; Crooks, R. M. Comparison of Nanoparticle Size and Electrophoretic Mobility Measurements Using a Carbon-Nanotube-Based Coulter Counter, Dynamic Light Scattering, Transmission Electron Microscopy, and Phase Analysis Light Scattering. *Langmuir* **2004**, *20*, 6940–6945.
9. Deblois, R. W.; Bean, C. P.; Wesley, R. K. A. Electrokinetic Measurements with Submicron Particles and Pores by Resistive Pulse Technique. *J. Colloid Interface Sci.* **1977**, *61*, 323–335.
10. Harms, Z. D.; Mogensen, K. B.; Nunes, P. S.; Zhou, K. M.; Hildenbrand, B. W.; Mitra, I.; Tan, Z. N.; Zlotnick, A.; Kutter, J. P.; Jacobson, S. C. Nanofluidic Devices with Two Pores in Series for Resistive-Pulse Sensing of Single Virus Capsids. *Anal. Chem.* **2011**, *83*, 9573–9578.
11. Ito, T.; Sun, L.; Crooks, R. M. Simultaneous Determination of the Size and Surface Charge of Individual Nanoparticles Using a Carbon Nanotube-Based Coulter Counter. *Anal. Chem.* **2003**, *75*, 2399–2406.
12. Berge, L. I.; Feder, J.; Jossang, T. A Novel Method To Study Single-Particle Dynamics by the Resistive Pulse Technique. *Rev. Sci. Instrum.* **1989**, *60*, 2756–2763.
13. Golibersuch, D. C. Observation of Aspherical Particle Rotation in Poiseuille Flow *via* the Resistance Pulse Technique. *Biophys. J.* **1973**, *13*, 265–280.
14. Platt, M.; Willmott, G.; Lee, G. U. Resistive Pulse Sensing of Analyte-Induced Multicomponent Rod Aggregation Using Tunable Pores. *Small* **2012**, 10.1002/smll.201200058.
15. Holden, D. A.; Hendrickson, G.; Lyon, L. A.; White, H. S. Resistive Pulse Analysis of Microgel Deformation during Nanopore Translocation. *J. Phys. Chem. C* **2011**, *115*, 2999–3004.
16. Qin, Z. P.; Zhe, J. A.; Wang, G. X. Effects of Particle's Off-Axis Position, Shape, Orientation and Entry Position on Resistance Changes of Micro Coulter Counting Devices. *Meas. Sci. Technol.* **2011**, *22*, 045804.
17. Rodriguez-Trujillo, R.; Castillo-Fernandez, O.; Garrido, M.; Arundell, M.; Valencia, A.; Gomila, G. High-Speed Particle Detection in a Micro-Coulter Counter with Two-Dimensional Adjustable Aperture. *Biosens. Bioelectron.* **2008**, *24*, 290–296.
18. Sowerby, S. J.; Broom, M. F.; Petersen, G. B. Dynamically Resizable Nanometre-Scale Apertures for Molecular Sensing. *Sens. Actuators, B* **2007**, *123*, 325–330.
19. Yusko, E. C.; Johnson, J. M.; Majd, S.; Prangkio, P.; Rollings, R. C.; Li, J.; Yang, J.; Mayer, M. Controlling Protein Translocation through Nanopores with Bio-Inspired Fluid Walls. *Nat. Nanotechnol.* **2011**, *6*, 253–260.
20. Roberts, G. S.; Kozak, D.; Anderson, W.; Broom, M. F.; Vogel, R.; Trau, M. Tunable Nano/Micropores for Particle Detection and Discrimination: Scanning Ion Occlusion Spectroscopy. *Small* **2010**, *6*, 2653–2658.
21. Vogel, R.; Willmott, G.; Kozak, D.; Roberts, G. S.; Anderson, W.; Groenewegen, L.; Glossop, B.; Barnett, A.; Turner, A.; Trau, M. Quantitative Sizing of Nano/Microparticles with a Tunable Elastomeric Pore Sensor. *Anal. Chem.* **2011**, *83*, 3499–3506.
22. Roberts, G. S.; Yu, S.; Zeng, Q.; Chan, L. C. L.; Anderson, W.; Colby, A. H.; Grinstaff, M. W.; Reid, S.; Vogel, R. Tunable Pores for Measuring Concentrations of Synthetic and Biological Nanoparticle Dispersions. *Biosens. Bioelectron.* **2012**, *31*, 17–25.
23. Willmott, G. R.; Vogel, R.; Yu, S. S. C.; Groenewegen, L. G.; Roberts, G. S.; Kozak, D.; Anderson, W.; Trau, M. Use of Tunable Nanopore Blockade Rates To Investigate Colloidal Dispersions. *J. Phys.: Condens. Matter* **2010**, *22*, 454116.
24. Vogel, R.; Anderson, W.; Eldridge, J.; Glossop, B.; Willmott, G. A Variable Pressure Method for Characterizing Nanoparticle Surface Charge Using Pore Sensors. *Anal. Chem.* **2012**, *84*, 3125–3131.
25. Kozak, D.; Anderson, W.; Grevett, M.; Trau, M. Modeling Elastic Pore Sensors for Quantitative Single Particle Sizing. *J. Phys. Chem. C* **2012**, *116*, 8554–8561.
26. Lan, W.-J.; Holden, D. A.; Zhang, B.; White, H. S. Nanoparticle Transport in Conical-Shaped Nanopores. *Anal. Chem.* **2011**, *83*, 3840–3847.
27. Heins, E. A.; Siwy, Z. S.; Baker, L. A.; Martin, C. R. Detecting Single Porphyrin Molecules in a Conically Shaped Synthetic Nanopore. *Nano Lett.* **2005**, *5*, 1824–1829.
28. Maxwell, J. C. *Treatise on Electricity and Magnetism*; Cambridge University Press: Cambridge, 1893; Vol. 2.
29. Lan, W.-J.; Holden, D. A.; Liu, J.; White, H. S. Pressure-Driven Nanoparticle Transport across Glass Membranes Containing a Conical-Shaped Nanopore. *J. Phys. Chem. C* **2011**, *115*, 18445–18452.
30. Firnkes, M.; Pedone, D.; Knezevic, J.; Doblinger, M.; Rant, U. Electrically Facilitated Translocations of Proteins through Silicon Nitride Nanopores: Conjoint and Competitive Action of Diffusion, Electrophoresis, and Electroosmosis. *Nano Lett.* **2010**, *10*, 2162–2167.